Wave-packet dynamics of noninteracting ultracold bosons in an amplitude-modulated parabolic optical lattice

Tomotake Yamakoshi and Shinichi Watanabe
Department of Engineering Science, University of Electro-Communications, 1-5-1 Chofugaoka, Chofu-shi, Tokyo 182-8585, Japan
(Received 29 September 2014; revised manuscript received 31 January 2015; published 12 June 2015)

The recent Aarhus experiment [Phys. Rev. A **88**, 023620 (2013)] produced wave packets by applying amplitude modulation to a trapped Bose–Einstein condensate (BEC) of ^{87}Rb using an optical lattice. The present paper renders a theoretical account of this experimental production of wave packets and their subsequent time evolution, focusing on a one-dimensional noninteracting bosonic system as a fundamental starting point for accurate quantum analysis. Since experimental manipulation requires efficient wave-packet creation, we introduce the "single-Q Rabi model" to give a simple and reliable description of the interband transition. As a natural extension, we demonstrate enhancement of the wave-packet production by the "two-step Rabi oscillation method" using either one or two frequencies. The subsequent time evolution is affected by the intertwining of Bragg reflection and the Landau–Zener transition at each band gap, which is analyzed with the aid of a semiclassical theory [Phys. Rev. Lett. **110**, 085302 (2013)].

DOI: 10.1103/PhysRevA.91.063614 PACS number(s): 03.75.Lm, 37.10.Jk, 67.85.−d

I. INTRODUCTION

Ultracold atoms in the optical lattice (OL) [1] have been eagerly studied since the experimental realization of Bose–Einstein condensates [2] and quantum degenerate Fermi gases [3]. Their high controllability and visibility render the systems suitable for the investigation of quantum vortices [4], force detectors [5], quantum simulators [6], artificial gauge fields [7], and so forth. In particular, a great deal of attention has been drawn to the Bose–(Fermi–)Hubbard model [8,9], which revealed a plethora of novel quantum phases such as appear in the Mott insulator superfluid transition [10] in relatively deep OL potentials. In contrast, the dynamics of ultracold atoms in rather shallow OLs may be interpreted by analogy to the valence electrons in crystals.

Experiments employ square-shaped pulse modulation of the OL amplitude to selectively excite atoms in specific quasimomentum states. The energy-band structure, a general consequence of the periodic potential, naturally plays an important role in coherent manipulation of the matter waves at band edges via the Bragg reflection and the Landau–Zener (LZ) transition. Consider a matter wave moving in a particular band under the influence of an external potential. The Bragg reflection causes the mean position of the matter wave to oscillate; namely, the Bloch oscillation [11], which is indeed observed in the presence of a constant force [12] and may be used to measure the gravitational acceleration g [13]. The LZ transition often occurs in the context of an anticrossing between two quasidegenerate adiabatic states which, in the present quasiperiodic system, correspond to a pair of adjacent bands at band edges. LZ transitions may be used to measure the lattice height [14] and for bifurcating matter wave packets [15].

Recently, there has been a revival of interest in atoms in combined potentials created by parabolic traps and optical lattices (parabolic OL hereafter). One interesting feature of the OL is that some of the eigenstates can be made spatially localized far away from the center of the parabolic trap [16–20]. These spatially localized eigenstates (referred to as SLEs) are candidates for quantum registers [21], for instance, with unprecedented precision. Moreover, the SLEs may help realize the Bose–Hubbard model by controlled access and allow us to investigate novel quantum phases such as the supersolid state [22].

The recent BEC experiment done in Aarhus [23] first excites a BEC by lattice amplitude modulation and thus creates wave packets in a higher energy band. Then, after a few milliseconds of free propagation, the atoms are deexcited by a second amplitude modulation at such a timing that the final wave packets are concentrated in the desired spatial regions where the trap and OL are energetically balanced. This situation is similar to the pump-dump (probe) technique in the field of atom optics which is used in the formation of ultracold ground-state molecules starting from loosely bound Fano–Feshbach molecules [24]. An important focus of the present paper is thus the optimization of population transfer to specific states. However, no satisfactory theoretical analysis exists for the parabolic OL system in situations where the net excitation energy exceeds the height of OL. Experimentally realized systems being quasi one dimensional (1D) in the sense that the OL and parabolic potential are aligned, we consider noninteracting bosonic systems in a one-dimensional parabolic OL in this paper.

Some early studies of the transfer process [25] by amplitude modulation indicate the presence of Rabi-type oscillatory behavior in the transition probability. It turns out that the interband population transfer is indeed governed by the coupled equations akin to those for Rabi oscillations in quantum optics. This analogy motivates us to borrow technical terms freely from quantum optics as though the lattice modulation were equivalent to irradiation of an atom by a laser beam. On the basis of this argument, we demonstrate that a sequential two-step excitation with two different frequencies is more efficient than with one frequency. Moreover, a most enlightening result of our investigation is that a simple Rabi model adapted to the Bloch energy-band structure is unexpectedly reliable. Technical details of this model are given in Appendix A. A well-designed use of the Rabi oscillation could thus be exploited for the desired optimization of the transfer process (Sec. III A).

From Sec. III B onward, we focus on the influence of the parabolic potential after the lattice modulation is turned off. The excited wave packet gets accelerated while still subjected to the dispersion relation governed by the OL. The Bragg reflection and the Landau–Zener transition continue to play an important role. Here we find the parabolic potential causes the position-dependent LZ transition whereas the linear potential such as the gravitational acceleration is known to cause the position-independent LZ transition. We employ the extended semiclassical theory originally applied to fermions in a parabolic OL in Ref. [26] for the present bosonic system and treat the Bragg reflection and the LZ transition in Sec. III B for comparison with the quantum results.

The paper is organized as follows: Section II outlines the system and its theoretical model, and some additional background about the experiment. Section III discusses the population transfer with single- and two-frequency excitations largely on the basis of our numerical results. Section III A introduces our "single-Q Rabi model" and analyzes the dynamics of the wave packet subject to the amplitude modulation. Section III B focuses on the LZ transition using classical mechanics for a simple estimate of the transition rate as well as for interpretation. Under a special condition, the LZ transition can lead to the loss of the wave packet's amplitude in a quasicontinuum energy band. Discussions of such "collapse" of the wave packet during a free propagation are given in Appendix B as a technical topic. Section IV concludes the paper.

This paper uses the recoil energy $E_r = \hbar^2 k_r^2/(2m)$ for the unit of energy, the recoil momentum $k_r = 2\pi/\lambda$ for the unit of (quasi) momentum, the lattice constant $a = 2/\lambda$ for the unit of length, and rescaled time $t = E_r t'/\hbar$ for the unit of time. Here $\hbar$, λ, and m correspond to the Planck constant, the wavelength of the optical lattice, and the mass of the particle, respectively.

II. SYSTEM IN COMBINED POTENTIAL OF OPTICAL LATTICE AND PARABOLIC TRAP

We begin with the description of the model time-dependent Hamiltonian $H = -\frac{\hbar^2}{2m}\frac{\partial^2}{\partial x^2} + V_0 \sin^2(k_r x)[1 + \epsilon_0 \cos(\omega' t')] + \frac{1}{2}m\omega_0^2 x^2$ where V_0, ϵ_0, ω', and ω_0 denote the height of the optical lattice, the modulation amplitude, the excitation frequency, and the frequency of the parabolic potential, respectively [16,18–20]. It can be cast into the following rescaled Hamiltonian:

$$H = -\frac{\partial^2}{\partial y^2} + s\sin^2(y)[1 + \epsilon_0 \cos(E_\omega t)] + \nu y^2$$
$$= H_0 + s\sin^2(y)\,\epsilon_0 \cos(E_\omega t), \quad (1)$$

where y, s, E_ω, and ν denote $y = k_r x$, $s = V_0/E_r$, $E_\omega = \hbar\omega'/E_r$, $\nu = m\omega_0^2/(2E_r k_r^2)$, and $H_0 = -\frac{\partial^2}{\partial y^2} + s\sin^2(y) + \nu y^2$, respectively.

In order to grasp the general characteristics of the system, let us observe the distribution of the static eigenstates of H_0 on a broad energy scale. Figure 1(a) is a "position" representation of eigenstates lying below $30E_r$. Because the trap potential varies very gradually as a function of y, it affects the periodicity of the OL slowly; the energy-band structure changes only adiabatically. The periodicity thus plays the major role in

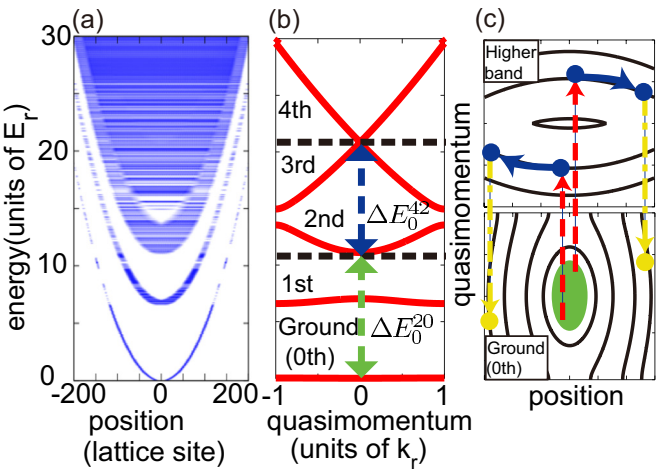

FIG. 1. (Color online) (a) Eigenenergies of time-independent Hamiltonian H_0 in the range of 0 to $30E_r$ represented in correlation with position space. The probability density of each eigenfunction is shade coded here as a function of coordinate y while the vertical location corresponds to its eigenenergy. The darker the shade, the higher the probability density. We note that the ground-state energy is set to 0 in what follows. (b) Energy-band structure of the uniform lattice system H_B. The energy difference at $q = 0$ between the ground and second bands ΔE_0^{20} (green arrow) and that between the second and fourth bands ΔE_0^{42} (blue arrow) serve as typical modulation frequencies in this article; specific values are $11.11E_r$ (30.4 kHz) and $9.82E_r$ (26.8 kHz), respectively. Panel (c) is a conceptual figure with the aid of the classical phase space showing how a specific state in the reduced-zone representation is reached from the ground state. Black solid lines are iso-energy contours in the specific bands. Initially, the atoms are localized at the center of the ground band, i.e., the green disk in the lower panel. The amplitude modulation (red dashed lines with arrows) creates the excited wave packets in a certain higher band (blue disks) and subsequently they move on the energy contour surface (blue solid lines with arrows). Likewise, it is possible to put wave packets into a certain higher or lower band by the second amplitude modulation with a suitable frequency (yellow chain lines).

governing the dynamics of the system. Let us recall the concept of quasimomentum in the uniform lattice system governed by $H_B = -\frac{\partial^2}{\partial y^2} + s\sin^2(y)$. The eigenstate corresponding to energy E_q^n is the Bloch state,

$$\phi_q^n(y) = e^{iqy}\sum_K C_B^n(K,q)e^{2iKy} \quad (n = 0,1,2,\ldots), \quad (2)$$

with suitable coefficients $C_B^n(K,q)$ where n, q, and $K \in \mathbb{Z}$ represent the band index, quasimomentum, and the corresponding reciprocal vector, respectively. Diagonalizing H_B in the basis of the Bloch states, Eq. (2), yields banded eigenenergies and coefficients. Let us call the lowest-energy band with index $n = 0$ the ground band hereafter.

With this background, let us briefly consider the coherent transfer process [23] with the aid of the classical phase-space maps in Fig. 1(c) in reduced-zone representation. (These maps actually derive from Eq. (3) below, including the trap potential, but are meant to serve as a conceptual guide here. They will serve as a computational tool in Sec. III B.) Here excitation is regarded as a jump from one map onto another.

First, the experiment superimposes the unidirectional optical lattice potential so slowly onto the parabolic trap that the ultracold atoms follow the deformation adiabatically and remain localized near the potential minimum [lower panel in Fig. 1(c)]. After this process, the height of the OL is modulated periodically [27] with respect to time to get the excited wave packet [upper panel in Fig. 1(c)]. The OL modulation couples states in different bands belonging to the same value of quasimomentum [28] as may be verified by a first-order perturbation analysis. Therefore, in the phase-space description in Fig. 1(c), the overlap in both position and quasimomentum plays an important role in population transfer.

The excited wave packet moves due to the parabolic potential whether the amplitude modulation is on or off. After the modulation is turned off, the following Hamiltonian in the single-band approximation [26] applies:

$$H(y,q) = E_q^n + \nu y^2. \tag{3}$$

The wave packet follows the energy contour in a specific band, and then the excitation or deexcitation with an appropriate delay time allows us to obtain the desired localized state. Roughly speaking, excitation with $E > s$ covers a wide range of position space, hence the excited wave packet lies in the quasicontinuum and can travel far to access an arbitrary state, once suitably deexcited. There stands an obstacle, however. There are band gaps even in the region where energy exceeds the height of the OL, thus causing collapse of the wave packet in addition to the natural dephasing. We analyze the LZ transition in Sec. III B.

III. NUMERICAL RESULTS AND DISCUSSIONS

References [25,29] used an amplitude-modulated optical lattice for exciting and probing cold trapped atoms. In the Aarhus experiment [23], ultracold bosonic atoms in the ground state were transferred to the fourth band via a two-photon process with a single modulation frequency, but optimization was not explored. The primary purpose of this section is to analyze the Aarhus data but, for a more noteworthy purpose, we consider how to optimize population transfer from the ground state to the fourth band not only with one frequency but also with two different frequencies. In accordance with the actual experiments using pulse-like modulation, here we consider the full time-dependent Hamiltonian, Eq. (1). In this paper, we fix the lattice height to $s = 16$, the parabolic trap strength to $\nu = 5.51 \times 10^{-5}$, and the modulation amplitude to $\epsilon_0 = 0.165$, respectively, as in the Aarhus experiment.

In the experiment, the excitation frequency employed lies in the vicinity of the energy difference between the bottom of the ground and second bands, i.e., ΔE_0^{20}; thus, we also investigate the same frequency region. On the other hand, Fig. 2 shows the band population as a function of modulation time comparing two excitation frequencies, $10.25E_r$ corresponding to an energy somewhat lower, and $11.35E_r$ somewhat higher than ΔE_0^{20}. From the figure, we extract the following two important facts:

(I) Figures 2(b) and 2(d) show clear-cut Rabi oscillations. Differences in excitation amplitude between the two frequencies reflect the degree of detuning. Such oscillations were observed in earlier experiments [25,27] and theoretically

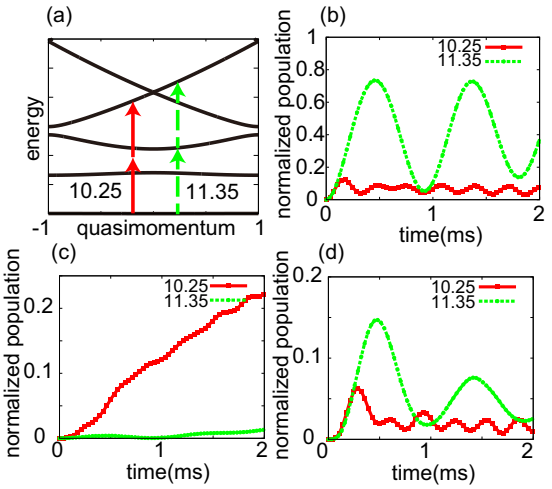

FIG. 2. (Color online) (a) A conceptual diagram for pumping the third band with $10.25E_r$ modulation in red and the fourth band with $11.35E_r$ modulation in green. Panels (b)–(d) show the resulting second-, third-, and fourth-band populations, respectively.

investigated [27], but without the parabolic trap. In addition, that the Rabi oscillations appear in Fig. 2(d) suggests the occurrence of two-photon processes.

(II) The band structure without the parabolic trap gives a reliable estimation of the targeted excitation, because the trap itself plays a passive role during the pulse-like excitation, being very loose. Indeed, it plays a preparatory role in the sense that the excitation process mainly occurs at the trap center where the ground state is localized.

We also note that more complicated behavior, involving direct, indirect, and higher-order processes, is found for the case shown in Fig. 2(c). The analysis of this behavior is complex and of sufficient interest that it will be published separately elsewhere.

According to (I), the amplitude-modulated system can be treated as if it were a "quantum optical" system. A by-product of this observation is the following approach of optimizing the fourth-band population by the two-step Rabi oscillation method with two different frequencies. The idea is to apply the second pulse at the moment the maximum amplitude of the second band is attained by the first pulse; that is, by a pair of π pulses with a well-chosen delay time. Due to the band structure, the second pulse frequency is chosen to be smaller than the 1st pulse, which inhibits the coupling between 0th and second bands. The green curve in Fig. 3 shows the result using the first pulse with energy $11.35E_r$, and then the second pulse with energy $10.25E_r$. The fourth band population is enhanced threefold by using this technique. This point is worthy of a special mention, particularly for experiment, since optimization of transfer can be greatly enhanced by this simple two-frequency excitation scheme. Manipulation at later stages becomes considerably easier with the enhanced transfer.

In what follows, we first analyze how these oscillations can be reproduced accurately by the single-Q Rabi model until the external field (in this case the trap) takes over. Second, we analyze the effect of the parabolic trap solely with a classical approach and see how the classical picture succeeds remarkably in interpreting its quantum counterpart.

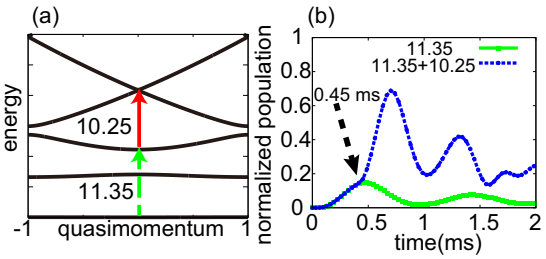

FIG. 3. (Color online) (a) A conceptual diagram for two-frequency excitation. The first pulse transfers the population from the ground to the second band with 0.45 ms modulation. Subsequently, the second pulse transfers from the second to the fourth band. (b) The fourth-band population with single-frequency modulation shown in red and two-frequency modulation with a suitable delay time in green, respectively. The two-frequency excitation leads to enhancement by a factor of three.

A. Interband transitions by single-Q Rabi model

Here we propose our single-Q Rabi model in order to account for the oscillations seen in full numerical calculations in Figs. 2 and 3. The model is based on time-dependent perturbation theory, treating the amplitude modulation as the perturbation term for the Bloch states in Eq. (2). This treatment gives an important fact that the perturbation term; namely, the Rabi frequency

$$\Omega_{nm}(q) = \epsilon_0 s\langle\phi_q^m|\sin^2(y)|\phi_q^n\rangle = \epsilon_0\left[\sum_K C_B^m(K,q)\,C_B^n(K,q)\,(q+K)^2\right], \quad (4)$$

couples two Bloch states in different bands, but only if the quasimomentum remains unchanged. The parabolic trap is ignored once the ground state is constructed around the minimum of the trapping potential.

Now, we represent the time-dependent wave function in terms of Bloch states as $\psi(y,t) = \sum_{n,q} C_Q^n(q,t)\phi_q^n(y)e^{-iE_\omega t}$. We consider the time evolution of the coefficients $\{C_Q^n(q,t)\}$. Their equation of motion reads

$$\frac{d}{dt}\begin{pmatrix} C_Q^0(q,t) \\ C_Q^2(q,t) \\ C_Q^3(q,t) \\ C_Q^4(q,t) \end{pmatrix} = -\frac{i}{2}\begin{pmatrix} 2\Delta_{02} & \Omega_{02} & 0 & 0 \\ \Omega_{02} & 0 & \Omega_{23} & \Omega_{24} \\ 0 & \Omega_{23} & -2\Delta_{23} & 0 \\ 0 & \Omega_{24} & 0 & -2\Delta_{24} \end{pmatrix} \times \begin{pmatrix} C_Q^0(q,t) \\ C_Q^2(q,t) \\ C_Q^3(q,t) \\ C_Q^4(q,t) \end{pmatrix}, \quad (5)$$

where the rotating wave approximation is employed. Here, the detuning $\Delta_{nm}(q,\omega) = (E_q^m - E_q^n) - E_\omega$ and the nth-band population B_n is given by $B_n(t) = \sum_q |C_Q^n(q,t)|^2$. The coupling matrix, Eq. (5), has the following features: First, the ground-state component couples strongly with only the second band via a one-photon process due to energy conservation. On the other hand, the second-band component couples with the ground state, third, and fourth bands. We thus retain the ground, second, third, and the fourth bands under the single-Q condition $\Delta q = 0$ while ignoring the 1st band entirely. See Appendix A for technical details.

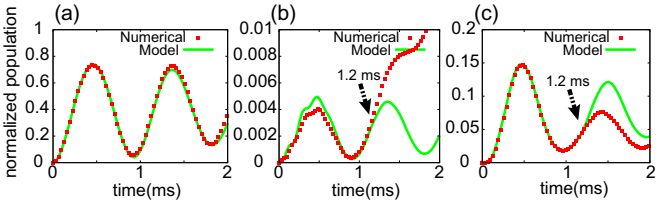

FIG. 4. (Color online) The band populations with $11.35E_r$ excitation as in Fig. 2. Panels (a)–(c) show the resulting second-, third-, and fourth-band populations, respectively. Solid curve and dots show the result of the Rabi model and direct numerical simulation, respectively. The model succeeds in reproducing the band populations closely until the LZ transition driven by the parabolic potential occurs at $t = 1.2$ ms in panels (b) and (c).

Figure 4 compares results of the single-Q Rabi model with those of direct numerical calculations for $11.35E_r$. The Rabi oscillations appear clearly in both results, and the agreement lasts for about two oscillations as in Figs. 4(b) and 4(c). This visible disagreement starting at $t = 1.2$ ms results from the acceleration due to the parabolic potential neglected in Eq. (5) which couples different q states and causes the excited wave packet to undergo a sudden change. Conversely, it suggests that the excited wave packet remains relatively narrow both in position and quasimomentum spaces up to the breakdown time. One interesting feature is that the numerical result of the third- and fourth-band populations departs from the model at almost the same time, one going up and the other going down. The moment $t = 1.2$ ms corresponds to the LZ transition at the narrow band gap between third and fourth band. However, in the presence of the amplitude modulation, it is difficult to isolate the transition between two neighboring bands. Therefore, let us consider the LZ transition quantitatively with the amplitude modulation turned off.

B. The Landau–Zener transition at band edges

In the current situation, the parabolic potential acts on each atom causing the LZ transition and/or the Bragg reflection at the band edge. To interpret the phenomenon at the third and fourth band gap, here we follow the dynamics of the fourth-band wave packet created with a pulse of energy $11.35E_r$ and duration of 0.45 ms. Figures 5(a) and 5(b) show the motion of the excited wave packet in position and quasimomentum spaces, respectively. Since the wave packet in quasimomentum space spreads symmetrically to either negative or positive values of q, the wave packet moves away from the center in either positive or negative direction almost linearly in time. (Note only the positive branch is shown here in the extended-zone representation with $3k_r < q < 4.5k_r$.) At about $t = 1.1$ ms later since the beginning of the free propagation, the wave packet in the fourth band crosses the boundary between the third and fourth bands [Fig. 5(a)]. At this moment, part of the wave packet suddenly changes its direction in position space [Fig. 5(b)] corresponding to the

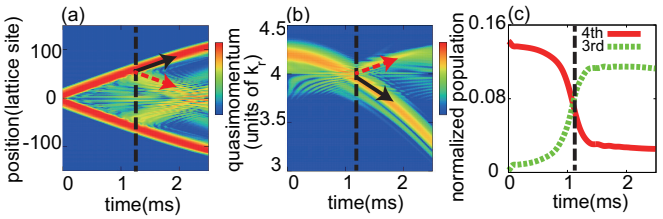

FIG. 5. (Color online) Free propagation of the excited wave packet after the pulse of energy $11.35E_r$ and duration of 0.45 ms is applied. Time $t = 0$ marks the end of the first excitation pulse. Time propagation in position and quasimomentum in extended-zone representation are shown in panels (a) and (b), respectively. Panel (c) represents the third- and fourth-band populations as a function of time.

Bragg reflection at the third-fourth band gap, and the other part goes to the third band due to the LZ transition. Figure 5(c) clearly shows a flow of population from the fourth to the third band due to the LZ transition.

Let us turn to the classical Hamiltonian, Eq. (3), for quantitative comparison. In this treatment, the classical particle moves along the constant-energy contour in phase space depicted in Fig. 6(b). Here the third and fourth bands are shown in extended-zone representation, but the others are suppressed [Fig. 6(a)]. When the classical atom reaches the Brillouin zone boundary $q_b = 4$ or -4, it either jumps to the other band by the LZ transition or stays in the same band by Bragg reflection. In order to estimate τ_c classically, assume that the classical atom at the fourth band is located at position $y = 0$ and quasimomentum $q = q_i$ as in Fig. 6 when the excitation pulse is turned off, and then it crosses the boundary $q_b = 4$ at

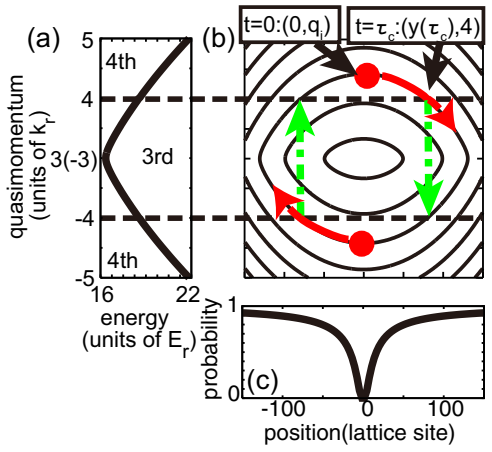

FIG. 6. (Color online) (a) Energy-dispersion relation within a limited region in partially-reduced-zone representation. Quasimomentum corresponds to the extended-zone representation, thus the dispersion curves are actually parted at $q = 3$ and $q = -3$ in extended-zone representation. (b) Iso-energetic lines represented in phase space. The classical trajectories move along these lines under the classical Hamiltonian, Eq. (3). Typical initial points in the fourth band (red circles) follow red solid arrows. When the classical point reaches the edge of the third or fourth band, the trajectory branches off, either going smoothly to the other band (red solid) or jumping to the other side (green dashed) of the same band by the Bragg reflection. (c) LZ transition rate between third and fourth bands shown as a function of position [Eq. (8)].

$t = \tau_c$. The initial quasimomentum q_i is estimated by the energy conservation of the direct two-photon excitation process, namely $E^4_{q_i} - E^0_{q_i} = 2E_\omega$. Once q_i is calculated, the critical time τ_c and the position at the critical time $y(\tau_c)$ are given by

$$\tau_c(q_i) = \frac{1}{2\sqrt{\nu}} \int_{q_b}^{q_i} \frac{1}{\sqrt{E^n_{q_i} - E^n_q}} dq, \tag{6}$$

and

$$y(\tau_c) = \sqrt{\frac{E^n_{q_i} - E^n_{q_b}}{\nu}}. \tag{7}$$

These formulas yield $\tau_c = 1.1$ ms and $y(\tau_c) = 177$ (corresponding to the 56th lattice site) with $q_i = 4.23$. These values are in good agreement with the numerical simulation in Figs. 5(a) and 5(b).

Next, we turn to the semiclassical estimation of the LZ transition rate. In accordance with the Zener's formula [30], the LZ transition rate is given approximately by

$$P_t(n, y) = \exp\left(-\frac{a_c(n)}{a(y)}\right) = \exp\left(-\frac{\pi\delta_n^2}{16n\nu|y|}\right), \tag{8}$$

where $a_c(n)$, $a(y)$, and δ_n represent the critical acceleration at the band gap, the acceleration at position y induced by the external potential, and the rescaled energy gap between the nth and $(n-1)$st band. It is worth pointing out that, in the case of the quadratic potential, the acceleration at the point of the crossing in quasimomentum depends on the position y whereas it does not in the case of a linear external potential such as gravity. Reading off the LZ transition rate from Fig. 5(c) as the ratio of the population of the third band at $t \gg 1.1$ ms to that of the fourth band at $t = 0$, we get roughly $P_t = 0.78$. This agrees with the value of 0.82 calculated by Eq. (8) to about 4% with $\delta_4 = 0.2$. We have also checked that the LZ transition rate in the case of two-color $11.35E_r + 10.25E_r$ excitation with 0.7 ms pulse duration. These formulas lead to $\tau_c = 0.58$ and $P_t = 0.68$ with $q_i = 4.07$. Additionally, it agrees with the numerically obtained LZ transition rate 0.71 to about the same accuracy. These representative examples confirm the validity of the present picture.

Making use of this classical approach, the breakdown time of the single-Q Rabi model due to the LZ transition can be easily estimated in systems with similar band structures. Let us close this section by noting that the LZ transition lowers the brightness of the wave packet, eventually leading to the collapse that takes place faster than with natural dephasing. A specific example is worked out in detail in Appendix B for the wave packet excited to a quasicontinuum such as the fourth band.

IV. CONCLUSIONS

We investigated the dynamics of ultracold bosonic atoms in a parabolic OL system for the major purpose of producing dense and robust wave packets. To this end, we studied the excitation process and subsequent dynamics of the excited wave packet with numerical simulations and a semi-analytical method.

We analyzed how the energy bands get populated during the production of wave packets. The intensity of the current

experimental amplitude modulation is actually very high, figuratively comparable to the laser acting on an atom so that multiphoton-type excitation can occur as in the so-called strongly coupled regime of the matter-light interaction. Thus, using the language of quantum optics, we introduced the single-Q Rabi model to account for the time dependence of the Bloch-band population. Although simple, the proposed model indeed showed good agreement with the rigorous numerical calculations. We also considered the two-frequency excitation procedure for enhancing wave-packet production in a most straightforward way; namely, with two successive π pulses separated in time such that the second pulse was applied right at the moment the intermediate state reached its maximum population by the first pulse. The confirmed enhancement factor reached about three for the demonstrated example; a very promising result.

We checked the subsequent dynamics and how the energy band gaps affect the wave packet. One feature we observed is that the relatively small gap behaves as an imperfect transmitter and causes the collapse of the wave packet. In this context, the well-known semiclassical formula for the LZ transition rate is verified to yield a reasonable estimate. An intriguing feature is that the LZ transition rate in the parabolic potential depends both on the position and band gap, thus specific values of the excitation parameters are affected by the LZ transition. Such complex manifestation of effects due to the band gaps suggests paradoxically that suitable control of the OL parameters may enable us to manipulate matter waves at will. For instance, Ref. [15] produces a chain of coherent wave packets via successive bifurcations.

The present analysis works very well with a quasi-1D system, i.e., the tight confinement in all but the direction of the OL. We now mention some aspects to be examined more closely in the future. The present treatment should be extended to a realistic three-dimensional system. Moreover, to analyze the real experiments, the experimental initial conditions need to be recreated. Such experimental knowledge is currently only incompletely available. In this work, we presumed the initial state to be the ground state at absolute zero temperature. Instead, we may theoretically simulate various initial states to infer the experimental initial condition. In addition to the dimensionality, the nonlinearity is an interesting issue as well [31]. We checked the previously reported comportment of the system [32] and verified that a weak nonlinearity in the mean-field approximation leads to stabilizing the wave packet via deformation of the classical separatrix. As the nonlinearity increases, the wave packet becomes irreparably unstable in a sudden manner.

The parabolic OL system is said to have a wide variety of applications, not limited to registering quantum information. In the case of fermionic atoms, the amplitude modulation can create particle-hole pairs in analogy with photoconductivity [26]. There is still much to be explored on the basis of the insights gained from the present linear system.

ACKNOWLEDGMENTS

This work was supported by JSPS KAKENHI Grant No. 26400416. T.Y. acknowledges support from the JSPS Institutional Program for Young Researcher Overseas Visits.

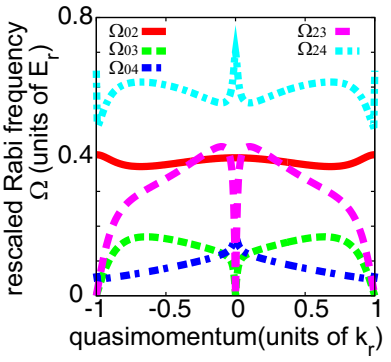

FIG. 7. (Color online) Rabi frequency $\Omega_{mn}(q)$ for transitions zeroth-second, zeroth-third, zeroth-fourth, second-third, and second-fourth. Note sharp peaks and dips at $q = 0$ caused by reflection symmetry.

We acknowledge Dr. Alexander Itin's vital contribution to this work with his useful suggestions throughout this study.

APPENDIX A: THE SINGLE-Q RABI MODEL

The model exploits the tight-binding Hamiltonian [17] for constructing the ground state of the parabolic OL. Usually, the eigenstates of the tight-binding Hamiltonian are expressed in terms of the spatially localized Wannier states. So, reexpressing the ground state in terms of the quasimomentum states of Eq. (2), we get

$$\chi_0(y) \cong \frac{1}{\sqrt[4]{\pi\alpha}} \sum_q e^{-q^2/2\alpha} \phi_q^0(y), \tag{A1}$$

where $\phi_q^0(y)$ is the ground-band Bloch state defined by Eq. (2) and $\alpha = [\nu/(\pi^2 J)]^{1/2}$. The approximation for the ground state is only valid when $\pi^2 J/\nu \gg 1$. Here the ground-band hopping parameter J is obtained by the approximate formula, Eq. (8) of Refs. [33,34]; namely, $J = \frac{4}{\sqrt{\pi}} s^{3/4} e^{-2\sqrt{s}}$ ($s \gg 1$). Therefore, the initial condition is $C_Q^0(q,0) = Ae^{-q^2/(2\alpha)}$, and the other coefficients are 0. The normalization coefficient A is $A = (\sum_q |e^{-q^2/\alpha}|)^{-1/2}$. The Rabi frequency thus strongly depends on the lattice depth s.

We comment on experimental parameter values before showing an illustrative example. Experimental groups working on the wave-packet creation and detection use rather similar parameter values [23,26]. All the values in this paper are from the Aarhus experiment [23] so that $s = 16$, $\nu = 5.51 \times 10^{-5}$, and $J = 6.06 \times 10^{-3}$. The Hamburg group varies ν and s; their representative values are $s = 10$, $\nu = 2.83 \times 10^{-5}$, and $J = 2.27 \times 10^{-2}$. Both experiments satisfy the condition $\pi^2 J/\nu \gg 1$, thus the single-Q Rabi model is applicable.

Figure 7 exhibits the Rabi frequency $\Omega_{nm}(q)$ for the relevant combinations of m and n. Since the initial-state distribution is concentrated near $q = 0$, we discuss the region $q \sim 0$. The Bloch coefficients $C_B^n(K,q)$ for the even (odd) band are symmetric (antisymmetric) with respect to K at $q = 0$. Therefore, at $q = 0$, the Rabi frequencies between even and odd bands are 0. This is nothing but the standard parity argument. This symmetry-based behavior is concentrated near $q = 0$ and then quickly taken over by the smoother averaged

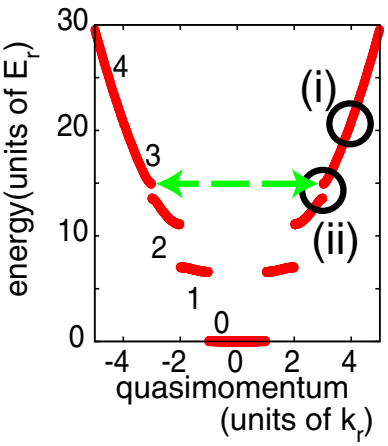

FIG. 8. (Color online) Energy-dispersion relation in extended-zone representation for $s = 16$. The encircled region (i) corresponds to the band gap between third and fourth $\sim 0.2E_r$ which is quite small. On the contrary, the band gap between second and third in the encircled region (ii) is $\sim 1.4E_r$ which is too large for the LZ transition. At (ii), we consider only the Bragg reflection schematically shown by the dashed green line joining the $q = -3$ and $q = 3$ states.

behavior. An important point is that Ω_{02} (red) and Ω_{24} (light blue) completely overcome Ω_{04} (blue) in the current situation. Therefore, the combined effect of Ω_{02} and Ω_{24} makes the population transfer faster and less susceptible to the acceleration due to the parabolic potential. The two-photon zeroth-fourth transfer rate is thus seen to be better than its single-photon counterpart. The single-Q Rabi model thus seems to provide a promising scheme of population transfer.

APPENDIX B: COLLAPSE OF WAVE PACKET DURING FREE PROPAGATION

A narrow band gap could serve simultaneously as a mirror and a beam splitter. The gap between the third and fourth bands for $s = 16$ is such a special case. We demonstrate the instability of the wave packet excited to the fourth band. Time evolution after the amplitude modulation is straightforward, the time dependence being given by $C_k(t) = C_k(0)e^{-iE_k t}$. Despite this simplicity, the wave-packet motion displays nontrivial features because of a large number of Bloch states involved.

We discuss dynamics of the wave packet excited to the fourth band in the manner of Sec. III B. Let us argue that the wave packet excited to the fourth band is confined in the third and fourth bands during free propagation in the case of $s = 16$ as seen in the Aarhus experiment [23]. Figure 8 shows the energy band in the extended-zone representation. The region marked (i) corresponds to the narrow gap between the third and fourth bands now located at $q = 4$. In contrast, the band gap between the second and third [region marked (ii)] is quite large, and the wave packet crosses the band edge of the second and third bands typically at $y = 300$; thus, we get a negligibly small LZ transition rate $P_t(n, y) = 6 \times 10^{-4}$ by Eq. (8). In addition, there holds the energy conservation, thus the wave packet can neither go to the lower bands nor to the higher bands.

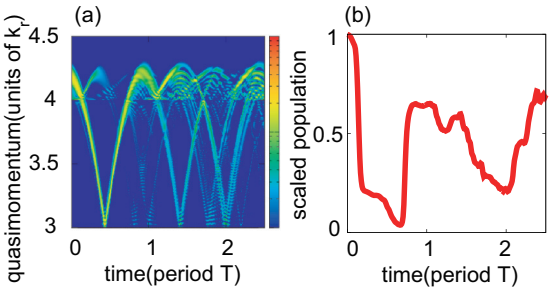

FIG. 9. (Color online) Free propagation after excitation by the $11.35E_r$ modulation. Panel (a) represents the quasimomentum distribution and panel (b) shows the fourth-band population in time. The y axis of panel (b) is scaled by the initial fourth-band population. Both figures show complicated structure after one period of oscillation due to the LZ transition.

As seen in Fig. 9(a), the excited wave packet with $11.35E_r$ excitation evolves into a very complicated structure in time. Let us define the time period T corresponding to the time for the wave packet to return to its initial quasimomentum $|q_i|$ after the first Bragg reflection at the second-third band edge. The wave packet bifurcates every time it reaches the band edge, thus the population at $t = mT$ is simply $P_t(n, y)^{2m}$ times the initial population [cf. Eq. (8) for the definition of $P_t(n, y)$]. The population estimated at $m = 1$ equals 64% which is in good agreement with the simulated fourth-band population [Fig. 9(b)]. However, the population reduction to 45% at $m = 2$ does not agree very well with a simple estimate possibly because of the more complex bifurcation sequence. The fact suggests that, from the viewpoint of creating dense and robust wave packets, the excitation to the bottom of the fourth band may not be advisable for $s = 16$.

[1] O. Morsch and M. Oberthaler, Rev. Mod. Phys. **78**, 179 (2006).
[2] M. H. Anderson, J. R. Ensher, M. R. Matthews, C. E. Wieman, and E. A. Cornell, Science **269**, 198 (1995); K. B. Davis *et al.*, Phys. Rev. Lett. **75**, 3969 (1995); C. C. Bradley, C. A. Sackett, J. J. Tollett, and R. G. Hulet, *ibid.* **75**, 1687 (1995).
[3] B. DeMarco and D. S. Jin, Science **285**, 1703 (1999).
[4] P. Vignolo, R. Fazio, and M. P. Tosi, Phys. Rev. A **76**, 023616 (2007).
[5] K. J. Hughes, J. H. T. Burke, and C. A. Sackett, Phys. Rev. Lett. **102**, 150403 (2009).
[6] M. Greiner, O. Mandel, T. Esslinger, T. W. Hänsch, and I. Bloch, Nature (London) **415**, 39 (2002).
[7] D. Jaksch and P. Zoller, New. J. Phys. **5**, 56 (2003).
[8] J. Hubbard, Proc. R. Soc. London, Ser. A **276**, 238 (1963).
[9] H. A. Gersch and G. C. Knollman, Phys. Rev. **129**, 959 (1963).
[10] T. Kimura, S. Tsuchiya, and S. Kurihara, Phys. Rev. Lett. **94**, 110403 (2005).

[11] F. Bloch, Z. Phys **52**, 555 (1929); C. Zener, Proc. R. Soc. London, Ser. A **145**, 523 (1934).
[12] O. Morsch, J. H. Müller, M. Cristiani, D. Ciampini, and E. Arimondo, Phys. Rev. Lett. **87**, 140402 (2001).
[13] H. Ott, E. de Mirandes, F. Ferlaino, G. Roati, G. Modugno, and M. Inguscio, Laser Phys., **15**, 82 (2005).
[14] M. Cristiani, O. Morsch, J. H. Müller, D. Ciampini, and E. Arimondo, Phys. Rev. A **65**, 063612 (2002).
[15] S. J. Park, H. K. Andersen, S. Mai, J. Arlt, and J. F. Sherson, Phys. Rev. A **85**, 033626 (2012).
[16] H. Ott, E. de Mirandes, F. Ferlaino, G. Roati, V. Turck, G. Modugno, and M. Inguscio, Phys. Rev. Lett. **93**, 120407 (2004).
[17] C. Hooley and J. Quintanilla, Phys. Rev. Lett. **93**, 080404 (2004).
[18] M. Rigol and A. Muramatsu, Phys. Rev. A **70**, 043627 (2004).
[19] A. M. Rey, G. Pupillo, C. W. Clark, and C. J. Williams, Phys. Rev. A **72**, 033616 (2005).
[20] M. Valiente and D. Petrosyan, Europhys. Lett. **83**, 30007 (2008).
[21] L. Viverit, C. Menotti, T. Calarco, and A. Smerzi, Phys. Rev. Lett. **93**, 110401 (2004).
[22] V. W. Scarola and S. Das Sarma, Phys. Rev. Lett. **95**, 033003 (2005).
[23] J. F. Sherson *et al.*, New J. Phys. **14**, 083013 (2012); P. L. Pedersen *et al.*, Phys. Rev. A **88**, 023620 (2013).
[24] C. P. Koch, E. Luc-Koenig, and F. Masnou-Seeuws, Phys. Rev. A **73**, 033408 (2006).
[25] M. C. Fischer, K. W. Madison, Qian Niu, and M. G. Raizen, Phys. Rev. A **58**, R2648 (1998).
[26] J. Heinze *et al.*, Phys. Rev. Lett. **110**, 085302 (2013).
[27] J. H. Denschlag *et al.*, J. Phys. B **35**, 3095 (2002).
[28] B. Hundt, Diploma thesis, Universität Hamburg, 2011 (unpublished).
[29] T. Stöferle, H. Moritz, C. Schori, M. Köhl, and T. Esslinger, Phys. Rev. Lett. **92**, 130403 (2004); D. Greif, L. Tarruell, T. Uehlinger, R. Jördens, and T. Esslinger, *ibid.* **106**, 145302 (2011).
[30] C. Zener, Proc. R. Soc. London, Ser. A **173**, 696 (1932).
[31] M. Jona-Lasinio *et al.*, Phys. Rev. Lett. **91**, 230406 (2003).
[32] J. Brand and A. R. Kolovsky, Eur. Phys. J. D **41**, 331 (2007).
[33] W. Zwerger, J. Opt. B: Quantum Semiclassical Opt. **5**, S9 (2003).
[34] J. Heinze *et al.*, Phys. Rev. Lett. **107**, 135303 (2011).